Monthly Notices
of the
ROYAL ASTRONOMICAL SOCIETY

MNRAS **486,** 851–867 (2019)
Advance Access publication 2019 March 27

doi:10.1093/mnras/stz898

Milky Way globular clusters in γ-rays: analysing the dynamical formation of millisecond pulsars

Raniere de Menezes,★ Fabio Cafardo★ and Rodrigo Nemmen★

Departamento de Astronomia, Instituto de Astronomia, Geofísica e Ciências Atmosféricas, São Paulo, Universidade de São Paulo, SP 05508-090, Brazil

Accepted 2019 March 25. Received 2019 February 21; in original form 2018 November 13

ABSTRACT

Globular clusters (GCs) are evolved stellar systems containing entire populations of millisecond pulsars (MSPs), which are efficient γ-ray emitters. Observations of this emission can be used as a powerful tool to explore the dynamical processes leading to binary system formation in GCs. In this work, 9 yr of *Fermi* Large-Area Telescope data were used to investigate the γ-ray emission from all GCs in the Milky Way. Twenty-three clusters were found as γ-ray bright, with two of them never having been reported before. It was also found that magnetic braking probably has a smaller impact on the formation rate of binary systems in metal-rich GCs than previously suggested, while a large value for the two-body encounter rate seems to be a necessary condition. The influence of the encounter rate per formed binary was for the first time explored in conjunction with γ-ray data, giving evidence that if this quantity is very high, binary systems will get destroyed before having time to evolve into MSPs, thus decreasing the total number of MSPs in a GC. No extended emission was found even for clusters whose optical extent is $\approx 0.5^{\circ}$; all of them are point-like sources spatially in agreement with the optical cores of the GCs, supporting previous X-ray results of heavier objects sinking into the clusters' cores via dynamical friction. The possibility of extrapolating these results to ultra-compact dwarf galaxies is discussed, as these systems are believed to be the intermediate case between GCs and dwarf galaxies.

Key words: globular clusters: general – pulsars: general – gamma-rays: general.

1 INTRODUCTION

Since the first detection of γ-rays from 47 Tucanæ with the *Fermi* Large-Area Telescope (LAT) (Abdo et al. 2009), globular clusters (GCs) have become a new class of γ-ray source. Previous observations in the 1990s with the Energetic Gamma-ray Experiment (EGRET) aboard the Compton Gamma-ray observatory found no signal of γ-ray emission from these sources but resulted in important flux upper limits for more than a dozen of them (Michelson et al. 1994). By studying GCs in γ-rays, one can learn about the dynamical evolution of these systems, as well as the mechanisms behind the formation of their millisecond pulsar (MSP) populations.

The γ-ray emission from GCs is attributed to their large number of MSPs (Bednarek & Sitarek 2007; Abdo et al. 2010c; Freire 2012; Caraveo 2014), which are known to be efficient γ-ray emitters (Chen 1991; Harding, Usov & Muslimov 2005; Caraveo 2014). The recent detection of pulsed γ-ray emission from some GCs has further strengthened this connection (Freire et al. 2011; Johnson et al. 2013). The populations of MSPs in these systems,[1] as the descendants of low-mass X-ray binaries (LMXBs), are believed to be formed as a natural consequence of frequent stellar encounters (Pooley et al. 2003), with the high number density of stars within a GC providing an excellent laboratory to test scenarios for compact binary formation. Evidence favouring this dynamical origin, i.e. positive correlations between the cluster's γ-luminosity (L_γ) with its stellar encounter-rate (Γ) and with its metallicity ([Fe/H]) have been found in the past few years (Hui, Cheng & Taam 2010a; Hui et al. 2010b; Abdo et al. 2010c; Bahramian et al. 2013; Hooper & Linden 2016; Lloyd, Chadwick & Brown 2018). In interpretations of the former, the stars are assumed to be captured one by the other at a rate proportional to $\Gamma \propto \rho_0^{3/2} r_c^2$, where ρ_0 is the central luminosity density and r_c is the cluster core radius (Verbunt 2003b). In the latter, for a metal-rich cluster, magnetic braking can be more efficient, facilitating orbital decay in binary systems as well as a higher probability of MSP formation (Hui et al. 2010b; Tam, Hui & Kong 2016).

★ E-mail: raniere.m.menezes@gmail.com (RdeM); fabio.cafardo@usp.br (FC); rodrigo.nemmen@iag.usp.br (RN)

[1] List containing all known pulsars in GCs: https://www.naic.edu/ pfreire/GCpsr.html

In contrast with other pulsars, MSPs begin as spun-down neutron stars in binary systems where the companion star is massive enough to evolve into a giant and overflow the Roche limit of the system (Lorimer 2001). The neutron star is then spun-up and wakes up as a recycled pulsar by accreting matter and increasing angular momentum at the expense of the orbital angular momentum of the binary system (Alpar et al. 1982). Due to their weak surface magnetic fields, MSPs lose their larger store of rotational kinetic energy much more slowly than common pulsars (Lorimer et al. 2005), remaining luminous for up to billions of years. γ-ray photons are mainly produced in the magnetosphere of MSPs, where inverse Compton scattering, synchrotron and curvature radiation are the main physical processes behind this emission (Sturrock 1971; Harding, Tademaru & Esposito 1978; Arons 1983; Cheng, Ho & Ruderman 1986; Bednarek & Sitarek 2007).

This work presents an analysis of all globular clusters in the Milky Way (Harris 1996 – 2010 edition), using 9 yr of *Fermi* LAT data as an effort for detecting them and characterizing their γ-ray emission and MSP formation scenarios. The observations and cuts on *Fermi* LAT data are described in Section 2; followed by the light curve analysis and study of correlations between γ-ray emission, encounter rate, and metallicity, in Section 3. Section 4 discusses the influence of magnetic braking on the formation of MSPs and the possibility of extrapolating the results in this work to ultra-compact dwarf galaxies.

2 DATA SELECTION AND ANALYSIS

The sample analysed consists of all 157 known GCs in the Milky Way. For 25 of them, γ-ray emission was previously described in Acero et al. (2015), Hooper & Linden (2016), and Zhang et al. (2016), although four of these sources were not confirmed here (2MASS-GC02, M15, NGC 6342, and Pal6). Each GC treated here was observed with LAT during a 9-yr period ranging from August 5, 2008 to August 5, 2017 (MET 239587201 – 523584005). The data was analysed using *Fermi* Science Tools v10r0p5, *fermipy* python package v0.16.0 (Wood et al. 2017) and Pass 8 (Atwood et al. 2013), which present better energy and angular resolution as well as an increased effective area and energy range than its predecessor Pass 7.

Following standard procedures ,[2] data for each source was selected within a $12^\circ \times 12^\circ$ region-of-interest (ROI), centred on the GCs positions given in the GLOBCLUST catalogue (Harris 1996 – 2010 edition), with energies ranging between 100 MeV and 100 GeV divided into 12 logarithmically spaced energy bins. Photons with energies >100 GeV were not considered, as the spectra of MSPs frequently presents an exponential cutoff behaviour above only a few GeV (Abdo et al. 2010a). Sources included in the *Fermi* LAT Third Source Catalogue (3FGL – Acero et al., 2015) and lying up to 5° outside the ROIs were taken into account as well as all sources found with the *fermipy* function *find_sources (sqrt_ts_threshold=5.0, min_separation = 0.4)*. The number of new sources found with *find_sources ()* varied substantially depending on the adopted ROI: for ROIs lying close to the Galactic plane, a number of ∼20 new sources was common; for the other ROIs, the number of new sources was typically $\lesssim$ 10. In very few cases, a new source was found closer than 0.4° from the GC position (e.g.: Palomar 6 and Whiting 1). In these situations, a case-by-case approach was performed, manually including a new source to avoid contamination on the GC flux upper limit measurement. Only events belonging to the *Source* class were used (evclass = 128 and evtype = 3). The filters applied with *gtmktime* were DATA_QUAL > 0 and the recommended instrument configuration for science LAT_CONFIG = = 1. A zenith angle cut of 90° was applied to avoid contamination from the Earth limb. For modelling, the Galaxy and the extragalactic background emission, the Galaxy background model gll_iem_v06.fits and the isotropic spectral template iso_P8R2_SOURCE_V6_v06.txt were adopted.

All sources were investigated by means of binned likelihood analysis (*gtlike* tool – MINUIT algorithm). To quantify the significance among the detections, a test statistic (TS) was calculated, defined as $TS = 2(\mathcal{L}_1 - \mathcal{L}_0)$, where the term inside parentheses is the difference between the maximum log-likelihoods with ($\mathcal{L}_1$) and without ($\mathcal{L}_0$) modelling the source. The chosen criteria for detection was TS > 25, corresponding formally to a significance slightly above 4σ (Mattox et al. 1996). If the detected GC belonged to 3FGL, its spectrum was modelled according to its description there. If a detected GC was not included in 3FGL (post-3FGL clusters, from now on), its spectrum was modelled with a power-law. For all sources lying within a radius of 5° from the centre of the ROIs, the normalization parameter was left free to vary.

Point sources consistent with the optical centre of the GCs were added to the models for each GC in the analysed sample and a TS residuals map was constructed for each one of them. These residuals maps were used together with aperture photometry light curves to obtain a clean sample of GCs, where only sources with a clear indication for an isolated γ-ray point-like emission spatially coincident with the optical position of the cluster and presenting steady light curves were taken into account. All detections are described in Section 3, while the TS residuals maps and flux upper limits for all non-detected GCs are shown in Appendix.

The cases of NGC 6624 and M28 should be considered separately. Both GCs were originally described as γ-ray bright (Abdo et al. 2010c; Tam et al. 2011). Later, they were observed to host γ-ray pulsations (Freire et al. 2011; Johnson et al. 2013) and were catalogued as individual pulsars in 3FGL. When modelling both clusters, these catalogued pulsars were taken into account, with their normalizations left free to vary. After that, the clusters' emission laid below the detection threshold.

3 RESULTS

3.1 Detections

Among the 157 GCs, 23 presented γ-ray emission spatially coincident with the optical centre of the clusters. Another four clusters (2MASS-GC02, M15, NGC 6342 and Pal6) were previously described as γ-ray bright in literature, but in this work their significances were found to be below the adopted threshold of TS = 25; the results for these clusters are described in Appendix. The 23 detected clusters are shown in Table 1, which is segmented in three panels: the upper one shows the 15 GCs cataloged in 3FGL; the middle panel shows the post-3FGL clusters, and the last/bottom panel shows the new GCs candidates detected in this work.

[2] *Fermi* science tools and fermipy tutorials: https://fermi.gsfc.nasa.gov/ssc/data/analysis/scitools/ and http://fermipy.readthedocs.io/en/latest/quickstart.html

Table 1. Observations of 23 globular cluster candidates with *Fermi* LAT in an energy range from 100 MeV up to 100 GeV. The upper panel displays the 3FGL associations, the middle panel shows the post-3FGL associations and the bottom panel shows the new candidates for GC. The adopted spectral models (SM) are indicated on the second column, where *PL* = *PowerLaw* and *LP* = *LogParabola*. The computation of the luminosities was performed assuming isotropic γ-ray emission and using the distances available in the GLOBCLUST catalog.

Cluster	SM	Luminosity 10^{34}erg s^{-1}	Energy flux 10^{-12}er g cm^{-2}s^{-1}	TS
47 Tuc	LP	6.26 ± 0.19	25.81 ± 0.77	5604
Terzan5	LP	42.39 ± 1.54	74.41 ± 2.71	3854
M62	LP	8.96 ± 0.55	16.2 ± 0.99	1036
NGC 6388	LP	29.34 ± 1.24	25.01 ± 1.06	880
Ω Cent	LP	3.57 ± 0.26	11.03 ± 0.8	863
2MS-GC01	LP	8.89 ± 0.54	57.33 ± 3.46	731
NGC 6440	PL	25.64 ± 1.4	29.66 ± 1.62	518
NGC 6316	PL	22.38 ± 1.62	17.29 ± 1.25	276
NGC 6441	PL	27.37 ± 1.86	17.0 ± 1.16	331
NGC 6752	PL	1.02 ± 0.1	5.32 ± 0.54	149
NGC 6652	LP	4.19 ± 0.58	3.5 ± 0.48	129
M80	PL	7.10 ± 0.95	5.94 ± 0.79	92
NGC 2808	PL	4.89 ± 0.67	4.43 ± 0.61	81
NGC 6541	PL	3.34 ± 0.44	4.97 ± 0.66	78
NGC 6717	PL	1.76 ± 0.38	2.92 ± 0.64	31
Glimp01	PL	9.83 ± 1.29	46.54 ± 6.09	286
Glimp02	PL	8.6 ± 1.07	23.74 ± 2.96	98
NGC 6397	PL	0.35 ± 0.05	5.5 ± 0.79	64
NGC 6139	PL	8.22 ± 1.31	6.73 ± 1.07	59
M12	PL	0.88 ± 0.17	3.20 ± 0.61	43
M5	PL	1.52 ± 0.33	2.25 ± 0.49	31
M14	PL	3.17 ± 2.49	3.06 ± 2.4	29
M79	PL	3.61 ± 0.82	1.81 ± 0.41	26

3.1.1 *Fermi-LAT 8-yr source list*

Cross-checking the detections in this work with the ones available on the preliminary LAT 8-year Point Source List (FL8Y[3]), some differences are found. Six sources (2MASS-GC02, M92, NGC 362, NGC 6304, NGC 6342, and Terzan 1) associated to GCs in FL8Y are not significant detections in this work; and only one of the GCs detected in this work is not listed in FL8Y (M79). All of these clusters (with exception of Terzan 1) are very close to the detection threshold. The found differences may be related to the different likelihood method adopted in FL8Y (weighted likelihood[4]) and may vary depending on the analysed region. The clusters 2MASS-GC02, NGC 362, and Terzan 1, for instance, are located on very complicated regions of the sky with bright diffuse emission. Also, M92 and M79 are ∼1° apart from very bright sources. Future analyses including the 4th source catalogue of the *Fermi*-LAT (4FGL, in preparation) will benefit from a new Galactic diffuse γ-ray emission model based on Pass 8 data, allowing for better results.

3.2 Point-like sources

The spatial consistency between the γ-ray and optical/infrared emission for the firmly detected post-3FGL sources can be checked in Fig. 1, where the low-energy centres of the GCs are always coincident with the centres of the TS residuals maps. All maps have evidence for γ-ray emission with a maximum lying less than 0.15° (∼2 pixels) from their centrs. TS maps for 3FGL clusters are not shown here, as their emission is generally easily visible in their counts maps. The two new sources found in this work, M14 and M79, had their best-fitted positions obtained with the function *localize()*, available in *fermipy*, which found a γ-optical/infrared spatial separation within 1σ uncertainty radius for both cases (Table 2).

In order to test the accidental coincidence rate in the analysed sample, 200 pre-selected points in RA and Dec (blank fields) were randomly chosen in the sky with $|b| > 20°$ and being at least 1° apart from any known 3FGL source. These blank fields were analysed exactly in the same way as the main GCs analyses and on 4.5 per cent of them a poiÀnt source with TS above the threshold was detected. This value corresponds to an upper limit on the false-positive rate of the associations with GCs shown in Table 1 and should not be confused with the detection significance of the sources. The 3FGL clusters here were assumed to be truly associated to GCs and are not included in this false alarm association rate.

3.3 Extended source analysis

For Ω Centauri, 47 Tucanæ, and NGC 6397, the three γ-ray bright GCs with largest optical angular diameter ($\gtrsim 0.5°$), extended emission models were tested. The extended emission templates were created in two ways: with DSS optical maps available in NASA's SkyView[5] virtual telescope (McGlynn, Scollick & White 1998) and with 25 2D-Gaussian source templates with sizes ranging from 0.003° to 1°. For all tests, the likelihood ratio method favoured the point-like model instead of the extended emission models, which, in the most optimistic cases, presented TS values of only $TS_{ext} = 0.73$ for Ω Centauri ($R_{68} = 0.055 \pm 0.031$), $TS_{ext} = 0.38$ for 47 Tucanæ ($R_{68} = 0.033 \pm 0.022$), and $TS_{ext} = 0.00$ for NGC 6397 ($R_{68} = 0.003 \pm 0.080$). These results are in agreement with heavier objects sinking into the clusters' cores via dynamical friction (Fregeau et al. 2003), as both binaries and single MSPs are significantly more massive than typical stars in a GC. The same conclusion is reached from X-ray observations of 47 Tucanæ (Edmonds et al. 2003; Heinke et al. 2005), where the cluster's X-ray source population is highly concentrated in its core.

3.4 Light curves

The intrinsic variability of MSPs completely disappears when the observations span through time-scales much longer than the MSP typical revolution time. A light curve with bins of months is expected to be quiescent (Abdo et al. 2010c), where its variability is attributed only to statistical fluctuations. High levels of variability in a light curve with such time-scales are unlikely to be associated with a GC; they could nevertheless be due to a background active galactic nucleus.

To test for variability, aperture photometry light curves were created with *gtbin* for every single γ-ray GC. The results are shown in Fig. 2, where the data was binned in 3-month intervals, the chosen aperture radius was 1°, and the spectral index was kept fixed at 2. All light curves analysed presented quiescent behaviour, as expected for GCs, with all data points lying within the 2σ standard deviation level (blue band).

[3] https://fermi.gsfc.nasa.gov/ssc/data/access/lat/fl8y/

[4] https://fermi.gsfc.nasa.gov/ssc/data/access/lat/fl8y/FL8Y_description_v8.pdf

[5] https://skyview.gsfc.nasa.gov/current/cgi/query.pl

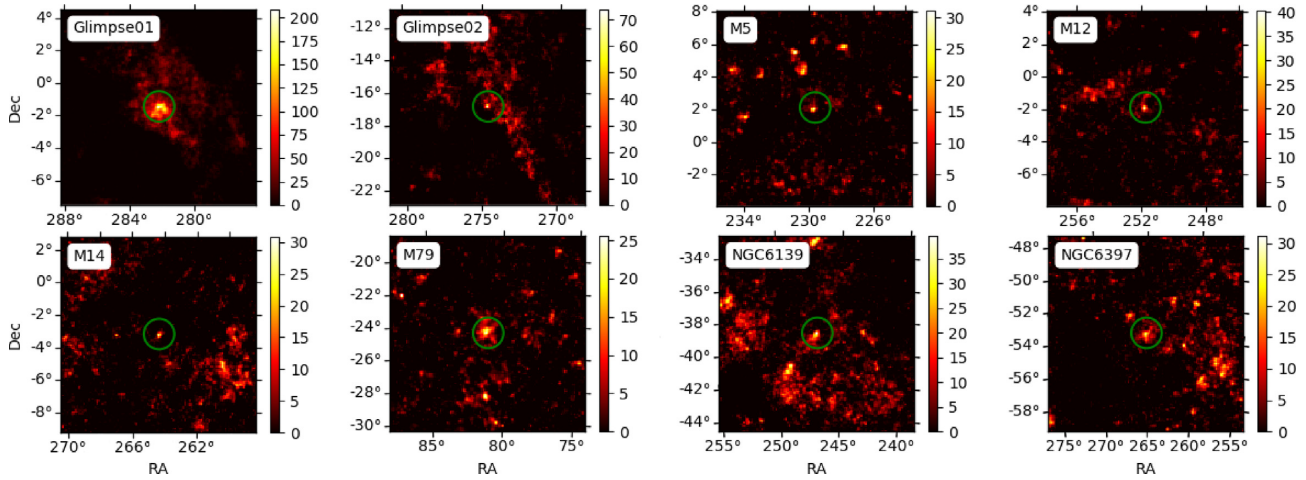

Figure 1. Mosaic of TS residuals maps for the firmly detected post-3FGL sources. These maps were generated with *tsmap()* function available in *fermipy*. The green circles guide the readers to the centre of the maps.

Table 2. Best-fit position for M14 and M79. $r_{1\sigma}$ is the 1σ error circle radius and α is the angular separation between the position of the γ-ray detection and the optical centre of the cluster. In both cases, α lies inside the 1σ uncertainty region. Positions are given in J2000 coordinates.

Cluster	RA	Dec	$r_{1\sigma}$	α
M14	264.412°	− 3.238°	0.035°	0.014°
M79	81.120°	− 24.410°	0.140°	0.134°

3.5 Spectral emission models

The high energy γ-ray spectra for 19 of the 23 detected GCs are shown in Fig. A3 in Appendix. All spectra are reasonably well fitted by a Logparabola or a power-law model, in agreement with the GCs discussed in Abdo et al. (2010c). As no significant deviation from such models is observed, the traditional interpretation that the γ-ray emission observed is coming from populations of MSPs was assumed throughout this work. Other models are discussed below.

One possible mechanism for producing γ-rays in GCs is inverse Compton scattering (ICS) by a relativistic population of electrons in the intracluster medium (Bednarek & Sitarek 2007). The spectra derived from such model, however, predict a hardening of the spectrum around 1–10 GeV (Bednarek & Sitarek 2007; Lloyd et al. 2018). In this work, no strong evidence for a spectral hardening was found in this band (Fig. A3).

Although dark matter annihilation has been proposed as another source of γ-rays in GCs (Brown et al. 2018), the lack of strong dynamical evidence (Moore 1996; Haşegan et al. 2005) suggests such processes cannot explain the majority of the γ-ray emission.

The results shown in Fig. 2 reduces the possibility of associating the observed γ-ray emission with cataclysmic variables within the clusters, as such sources are transient in nature (Abdo et al. 2010b) and no significant variability was observed in the analysed light curves.

3.6 Correlated quantities

Parameters such as the two-body encounter rate Γ and metallicity [Fe/H] are expected to influence the formation rate – and so the total number – of MSPs in a GC (see Section 1). For estimating the total number of MSPs, $N_{\rm MSP}$, within a cluster, a simple calculation was performed (Abdo et al. 2010c):

$$N_{\rm MSP} = \frac{L_\gamma}{\langle \dot{E} \rangle \langle \eta_\gamma \rangle}, \tag{1}$$

where L_γ is the cluster's isotropic γ-ray luminosity, $\langle \dot{E} \rangle$ is the average power emitted during the spin-down of MSPs, and $\langle \eta_\gamma \rangle$ is the average efficiency with which the spin-down power is converted into γ-ray luminosity. The isotropic energy luminosity was simply calculated as $L_\gamma = 4\pi r^2 \epsilon_\gamma$, where ϵ_γ is the measured energy flux (Table 1) and r is the distance to the cluster taken from Harris (1996; 2010 edition). The average spin-down power and average spin-down-to-γ-ray efficiency were adopted as $\langle \dot{E} \rangle = (1.8 \pm 0.7) \times 10^{34}$ erg s^{-1} and $\langle \eta_\gamma \rangle = 0.08$ for all clusters (Abdo et al. 2010c). These values were estimated from comparisons of the log $\dot{P}$ distributions of Galactic field MSPs with the accelerated corrected log $\dot{P}$ distribution for MSPs in 47 Tucanæ and by the average η_γ efficiency of the nearest MSPs to date as described in Abdo et al. (2009). Equation (1) is a rough estimate of L_γ, as in some cases L_γ may be dominated by the emission of a single MSP (Freire et al. 2011; Tam et al. 2011; Wu et al. 2013). Nevertheless, it should be good enough to at least establish an upper limit for the actual number of MSPs in a GC.

The scatter plots for $N_{\rm MSP}$ versus Γ and $N_{\rm MSP}$ versus [Fe/H] are shown in Fig. 3. For these plots, all γ-ray bright GCs with data values for metallicity and central luminosity density (needed for calculating Γ) available in the GLOBCLUST catalogue were used. Note that the encounter rate is in arbitrary units and was normalized such that $\Gamma = 100$ for M62, as done in Abdo et al. (2010c).

A simple linear least-squares regression was performed to the data displayed in Fig. 3. In the upper panel,

$$\log N_{\rm MSP} = a \log \Gamma + b \tag{2}$$

where $a = 0.64 \pm 0.15$, $b = 0.80 \pm 0.20$ with a mean deviation of the data about the model of $\Delta(\log N_{\rm MSP}) = 0.40$ dex and a Pearson correlation coefficient $P_{\rm corr}$ and p-value for testing non-correlation $p_{\rm n\text{-}c}$ of $P_{\rm corr} = 0.72$ and $p_{\rm n\text{-}c} = 0.00034$, respectively. In the bottom panel,

$$\log N_{\rm MSP} = a[{\rm Fe/H}] + {\rm b} \tag{3}$$

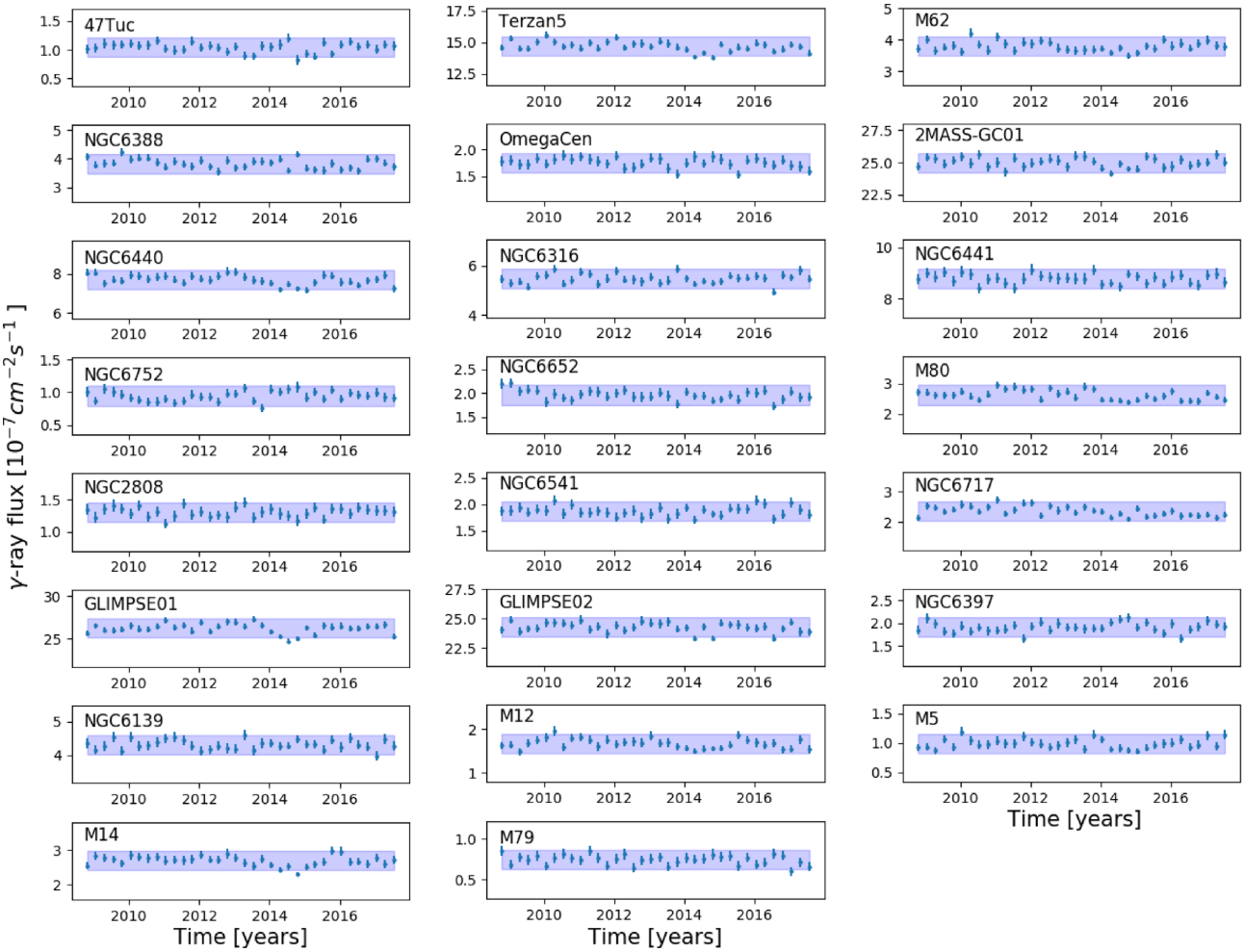

Figure 2. Aperture photometry light curves for the 23 γ-ray bright GC. Each bin corresponds to 3 months of data in an energy range from 100 MeV to 100 GeV and aperture radius of 1°. All sources exhibit weak variability, showing no flares with peaks significantly above the 2σ deviation level (blue band). None of the clusters were excluded from the analysed sample based on their light curves.

with $a = 0.76 \pm 0.14$, $b = 2.42 \pm 0.17$, $\Delta(\log N_{\rm MSP}) = 0.37$ dex, $P_{\rm corr} = 0.76$, and $p_{\rm n\text{-}c} = 0.000062$. Both correlations indicate that the γ-ray luminosity (or $N_{\rm MSP}$, since $N_{\rm MSP} \propto L_\gamma$) of a cluster increases with its Γ and/or metallicity.

To test if these correlations are valid for all GCs in the Milky Way, Fig. 4 shows the [Fe/H] $\times$ Γ scatter plot. As can be seen, all detected γ-ray clusters have a relatively large encounter rate, while their metallicities assume very dispersed values. This result may indicate that the magnetic braking effect is not significantly enhanced in metal-rich clusters, having a smaller role in the compact binary system formation rate than previously suggested (Hui et al. 2010b; Tam et al. 2016). Although the metallicity and the $N_{\rm MSP}$ (or L_γ) indeed present a correlation, as shown in Figs 3 and 5, the high metallicity may not be interpreted as causing the formation of MSPs (via magnetic braking). If the metallicity increased the MSP formation, then the detections (red dots) in Fig. 4 should be concentrated in the upper part of the plot. On the other hand, the presence of MSPs is an indicative of a past full of supernovae explosions, which could enhance the clusters' environments with metals (see Section 4 for a discussion).

A correlation between $N_{\rm MSP}$, Γ, and [Fe/H] in a plane was also explored in a 3D log space. Fig. 5 shows the fit from different angles. For testing its goodness of fit, a reduced chi-squared coefficient was calculated, giving $\chi^2_\nu = 2.67$. The plane is described by

$$\log N_{\rm MSP} = a[{\rm Fe/H}] + {\rm b}\log\Gamma + {\rm c} \quad (4)$$

where $a = 0.60 \pm 0.14$, $b = 0.39 \pm 0.12$, and $c = 1.78 \pm 0.27$, with a mean deviation of the data about the model of only $\Delta(\log N_{\rm MSP}) = 0.29$ dex. In comparison with the fits in Fig. 3, the scatter here is smaller, suggesting that a plane is a better description of the data. The advantage of displaying the data in this way is that once two low-energy observables are obtained (Γ and [Fe/H]), one can roughly constrain the γ-luminosity of a GC.

Planes relating L_γ with Γ and $u_{\rm sp}$ (the soft photon energy density), and with $[Fe/H]$ and $u_{\rm sp}$, were proposed in the past (Hui et al. 2010b), but the data used there was limited to less than 2 years of *Fermi*-LAT observations, resulting in high-dispersion plots.

3.7 Secondary encounters and binary disruption

Besides the observed correlation between $N_{\rm MSP}$ and Γ, there are some aspects of the formation and evolution of MSPs not described by Γ, like the effects caused by secondary encounters. Once the binary is formed, it may undergo subsequent encounters, which may disrupt the system or even exchange binary members.

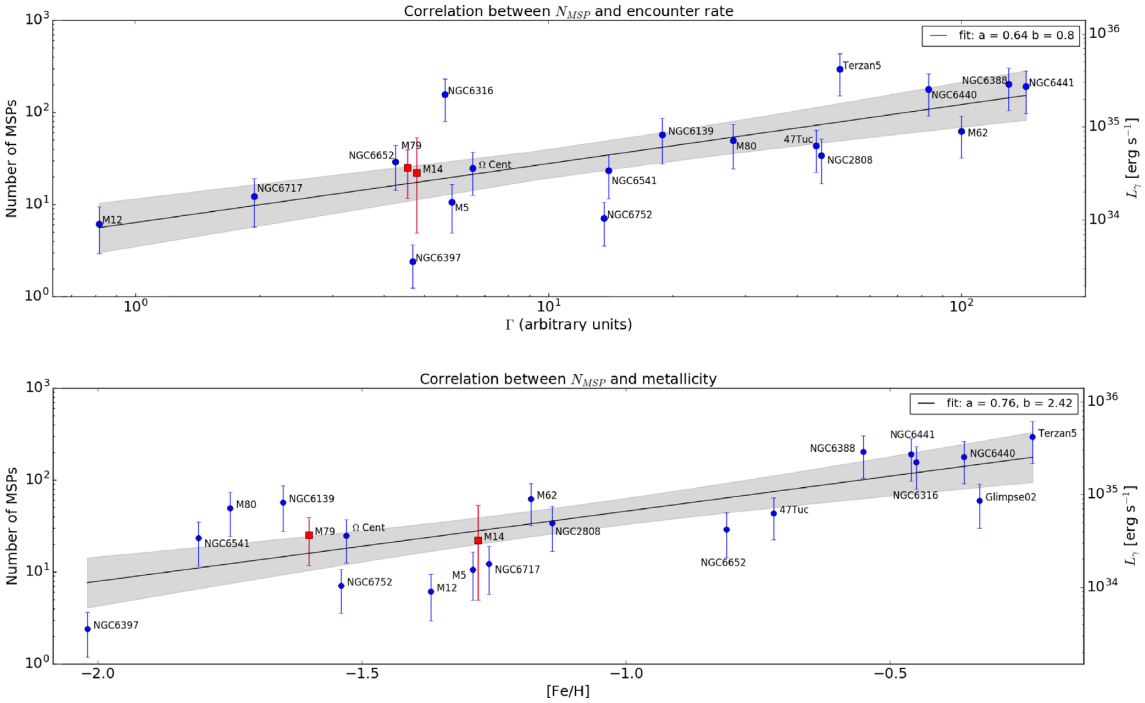

Figure 3. Correlation plots for $N_{\rm MSP} \times \Gamma$ and $N_{\rm MSP} \times [Fe/H]$ for the γ-ray bright GCs described in this work. The two new candidates for GCs found in this work are plotted as red squares. Sources lacking values of metallicity, central luminosity density, or cluster's core radius in GLOBCLUST catalogue were neglected. The shaded areas are the 1σ confidence bands. For a version of the upper panel plot including upper limits, see Appendix.

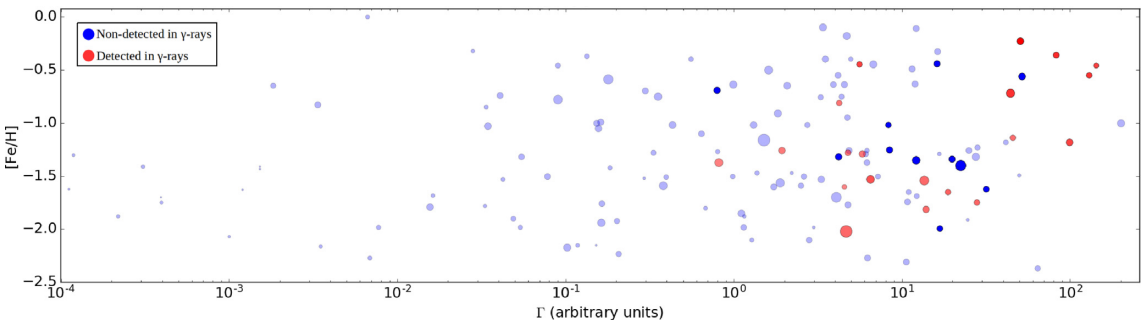

Figure 4. Influence of [Fe/H] and Γ for 143 GCs in the Milky Way (those for which metallicity and encounter rate can be taken or calculated from data available in GLOBCLUST). The size of each point scales with distance: the closer the cluster, the larger the point. *Blue points*: GCs non-detected by *Fermi*-LAT. Clusters with $\Lambda > 350$ are represented in dark blue. These sources are expected to be faint in γ-rays (see Section 3.7). *Red points*: GCs detected in γ-rays. In this case, the darker the point, the bigger the γ-ray energy flux. Detections are concentrated towards high values of encounter rate.

Analogously to the estimation of Γ described in Section 1, one can estimate the encounter rate per formed binary as $\Lambda \propto \sqrt{\rho_0}/r_c$ (Verbunt 2003a; Verbunt & Freire 2014), where ρ_0 and r_c are the central luminosity density and core radius, respectively. In GCs with large values for Λ, the lifetime of binaries should be relatively short ($\tau = 1/\Lambda$) before being disrupted or undergoing an exchange. The evolution of LMXBs in such clusters may be interrupted before their neutron stars become completely recycled, which may affect their overall population of MSPs. This behaviour is perhaps what is seen in Fig. 6, where a drop in $N_{\rm MSP}$ is evident for very large values of Λ (normalized such that $\Lambda = 100$ for M62). The high Λ values for NGC 6752 and NGC 6397 can also explain why these clusters have such low γ-ray luminosity and appear as outliers in Fig. 3.

Interestingly, GCs with intermediate values for Λ are those with the largest populations of MSPs (Fig. 6). This suggests that MSPs are preferentially formed in secondary exchange encounters, as only clusters with intermediate or high Λ are likely to host pulsar binaries formed in this way (Verbunt & Freire 2014).

High values for Λ may also be the explanation for many of the non-detections shown in Fig. 4. Many of the clusters with high Γ, which are roughly expected to be γ-ray bright, also have high Λ, which may negatively affect their MSP population. Non-detected clusters with $\Lambda > 350$ are plotted in dark blue in Fig. 4.

4 DISCUSSION

4.1 Connection between GCs and UCDs

Ultra-compact dwarf galaxies (UCDs) are a class of stellar system much brighter and more massive than typical globular clusters, but slightly more extended (Drinkwater et al. 2003). Similarities between both classes of objects are extensively discussed in literature

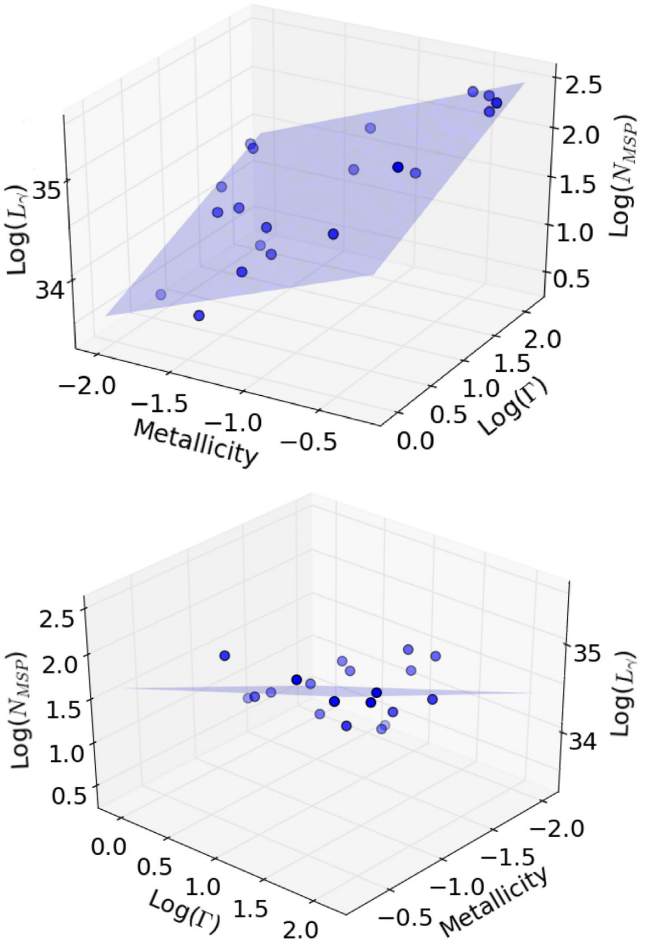

Figure 5. Fit of the plane $\log N_{\rm MSP} = 0.60 \times [{\rm Fe/H}] + 0.39 \times \log\Gamma + 1.78$ viewed from different angles.

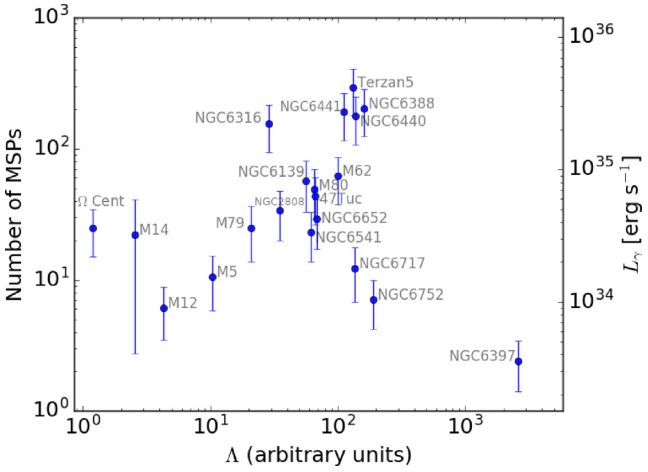

Figure 6. Impact of Λ on the populations of MSPs. The largest populations of MSPs are concentrated in clusters with intermediate values of Λ, indicating that MSPs are preferentially formed in secondary exchange encounters.

Table 3. UCD γ-ray energy fluxes and luminosities estimated by the encounter rate correlation described in the text. Fluxes are substantially below *Fermi*-LAT threshold.

UCD	Luminosity erg s^{-1}	Energy flux er g cm^{-2}s^{-1}	Γ	Distance Mpc
M59-UCD3	1.8×10^{35}	6.7×10^{-18}	123	∼15
M85-HCC1	13×10^{35}	34×10^{-18}	2848	∼18

(Mieske, Hilker & Infante 2002; Drinkwater et al. 2004; Forbes et al. 2008), where UCDs are treated as a link between GCs and dwarf galaxies, with the possible presence of dark matter in UCDs being the main difference between them (Haşegan et al. 2005). Taking advantage of these similarities, a tentative estimate of the γ-ray emission for a couple of UCDs was performed.

To have an idea of their γ-ray luminosities, some of the densest known UCDs were chosen: M59-UCD3 (Liu et al. 2015) and M85-HCC1 (Sandoval et al. 2015) and the $N_{\rm MSP} \times \Gamma$ correlation discussed in Section 3 was applied. Using their central luminosity densities and core radii (the core radius $r_{\rm core}$ was assumed here as $1/5 \times r_{\rm half}$, the half-light radius, which is very close to the mean value for the ratio $r_{\rm core}/r_{\rm half}$ in GLOBCLUST catalogue) given by Sandoval et al. (2015), their values for Γ and then L_γ were estimated (Table 3). Despite M85-HCC1 presenting a value for Γ beyond the fitted range of Fig. 3, it was assumed that the correlation was still valid at least as a first approximation. To estimate their energy fluxes, isotropic emission was assumed and the distances to M59 and M85 were taken from Blakeslee et al. (2009). Despite their high luminosity, these compact galaxies are so far away that their energy fluxes are extremely low, not detectable by the Fermi-LAT.

These estimations, although naive, may be important in the future when looking for very faint signals as, for example, dark matter annihilation lines in galaxy clusters crowded with UCDs, like Virgo (Jones et al. 2006) and Abell 1689 (Mieske et al. 2004), or even in individual dwarf elliptical galaxies. Searches like these were performed in recent years (Ackermann et al. 2010; Ando & Nagai 2012; Ackermann et al. 2015a,b) where interesting upper limits for dark matter annihilation models were found.

4.2 The driving mechanism behind MSP formation

In a scenario where the magnetic braking effect is significantly enhanced by a metal-rich environment, high γ-ray fluxes should be seen for clusters with high metallicities; but this is not observed in Fig. 4, which shows that metal-rich clusters are not necessarily efficient γ-ray emitters. This result suggests that a higher metallicity does not imply a significantly larger magnetic braking effect (and thus a higher MSP formation rate). Hypotheses for explaining the high metallicities in clusters crowded with MSP may be related to the feedback of MSPs or their progenitors within the clusters environment.

At least 5 of the 23 clusters described in this work (Ω Cen, NGC 2808, NGC 6397, NGC 6752 and M5) are abundant in Calcium (Lee et al. 2009). Calcium and other heavy elements can only be supplied to these systems via supernovae explosions (Timmes, Woosley & Weaver 1995). As the gravitational potential well in present-day clusters cannot retain most of the ejecta from such explosions (Baumgardt, Kroupa & Parmentier 2008), it has been suggested by Lee et al. (2009) that these GCs are most likely relics of what were once the nuclei of primordial dwarf galaxies accreted and disrupted by the Milky Way (Bica et al. 2006). This supernova enrichment hypothesis is also supported by some GCs formation models, where stellar winds and supernova ejecta within proto-GCs are decelerated to speeds below the clusters' escape velocity by the pressure of the surrounding hot gas in which they are embedded

(Brown, Burkert & Truran 1991). The metallicity of a cluster, in this context, is simply a function of its total number of supernovae (and not necessarily $N_{\rm MSP}$).

5 CONCLUSIONS

Nine years of *Fermi* LAT data were analysed, revealing GC candidates characterized by quiescent γ-ray emission spatially coincident with the optical centres of the clusters. The novelty of this work is mainly:

(i) Evidence that metallicity does not have a significant impact on the MSPs formation. If a metal-rich environment was one of the causes of MSP formation (enhancing the magnetic braking), a concentration of detections (red dots) should be seen in the upper part of Fig. 4. The results indicate that the MSP formation may be dominated by the encounter rate and encounter rate per binary rather than by an enhanced magnetic braking effect.

(ii) It was the first time that the encounter rate per formed binary (Λ) was analysed in conjunction with the γ-ray luminosity (Fig. 6). The resulting insight was that if Λ is very high, binary systems will get destroyed before having time to evolve into a MSP, so impacting the total number of MSPs in a GC.

(iii) The characterization of a clean sample of 23 γ-ray bright GC, where 2 of them (M14 and M79) have never been reported before, as well as upper limits on energy flux for all remaining GCs in the Milky Way.

(iv) No detected cluster presented extended emission; all of them are point-like sources spatially in agreement with the optical core of the GCs. It was confirmed (for the first time in γ-rays) the X-rays results of heavier objects sinking into the clusters' cores via dynamical friction.

ACKNOWLEDGEMENTS

We acknowledge useful discussions with Paulo C. C. Freire, Matthew Kerr, Philippe Bruel, Heitor Ernandes, Ana Chies Santos, and Beatriz Barbuy. We thank the anonymous referee for constructive comments which helped to improve the manuscript. This work was supported by CNPq (**Conselho Nacional de Desenvolvimento Científico e Tecnológico**) and FAPESP (Fundação de Amparo à Pesquisa do Estado de São Paulo, grants 2016/25484-9 and 2017/01461-2).

The *Fermi* LAT Collaboration acknowledges generous ongoing support from a number of agencies and institutes that have supported both the development and the operation of the LAT as well as scientific data analysis. These include the National Aeronautics and Space Administration and the Department of Energy in the United States, the Commissariat à l'Energie Atomique and the Centre National de la Recherche Scientifique/Institut National de Physique Nucléaire et de Physique des Particules in France, the Agenzia Spaziale Italiana and the Istituto Nazionale di Fisica Nucleare in Italy, the Ministry of Education, Culture, Sports, Science and Technology (MEXT), High-Energy Accelerator Research Organization (KEK) and Japan Aerospace Exploration Agency (JAXA) in Japan, and the K. A. Wallenberg Foundation, the Swedish Research Council, and the Swedish National Space Board in Sweden.

Additional support for science analysis during the operations phase is gratefully acknowledged from the Istituto Nazionale di Astrofisica in Italy and the Centre National d'Études Spatiales in France. This work performed in part under DOE Contract DE-AC02-76SF00515.

REFERENCES

Abdo A. et al., 2009, Science, 325, 845
Abdo A. et al., 2010a, ApJS, 187, 460
Abdo et al., 2010b, Science, 329, 817
Abdo A. et al., 2010c, A&A, 524, A75
Acero F. et al., 2015, ApJS, 218, 23
Ackermann M. et al., 2010, J. Cosmol Astropart. Phys., 2010, 025
Ackermann M. et al., 2015a, Phys. Rev. Lett., 115, 231301
Ackermann M. et al., 2015b, ApJ, 812, 159
Alpar M., Cheng A., Ruderman M., Shaham J., 1982, Nature, 300, 728
Ando S., Nagai D., 2012, J. Cosmol. Astropart. Phys., 2012, 017
Arons J., 1983, ApJ, 266, 215
Atwood W. et al., 2013, preprint (arXiv:1303.3514)
Bahramian A., Heinke C. O., Sivakoff G. R., Gladstone J. C., 2013, ApJ, 766, 136
Baumgardt H., Kroupa P., Parmentier G., 2008, MNRAS, 384, 1231
Bednarek W., Sitarek J., 2007, MNRAS, 377, 920
Bica E., Bonatto C., Barbuy B., Ortolani S., 2006, A&A, 450, 105
Blakeslee J. P. et al., 2009, ApJ, 694, 556
Brown J., Burkert A., Truran J. W., 1991, ApJ, 376, 115
Brown A. M., Lacroix T., Lloyd S., Bœhm C., Chadwick P., 2018, Phys. Rev. D, 98, 041301
Caraveo P. A., 2014, ARA&A, 52, 211
Chen K., 1991, Nature, 352, 695
Cheng K., Ho C., Ruderman M., 1986, ApJ, 300, 500
Drinkwater M. J., Gregg M. D., Hilker M., Bekki K., Couch W. J., Ferguson H. C., Jones J. B., Phillipps S., 2003, Nature, 423, 519
Drinkwater M. J., Gregg M. D., Couch W. J., Ferguson H. C., Hilker M., Jones J. B., Karick A., Phillipps S., 2004, PASA, 21, 375
Edmonds P. D., Gilliland R. L., Heinke C. O., Grindlay J. E., 2003, ApJ, 596, 1197
Forbes D. A., Lasky P., Graham A. W., Spitler L., 2008, MNRAS, 389, 1924
Fregeau J. M., Gürkan M., Joshi K., Rasio F., 2003, ApJ, 593, 772
Freire P. et al., 2011, Science, 334, 1107
Freire P. C., 2012, Proc. Intl. Astron. Union, 8, 243
Harding A. K., Tademaru E., Esposito L., 1978, ApJ, 225, 226
Harding A. K., Usov V. V., Muslimov A. G., 2005, ApJ, 622, 531
Harris W. E., 1996, AJ, 112, 1487
Haşegan M. et al., 2005, ApJ, 627, 203
Heinke C. O., Grindlay J. E., Edmonds P. D., Cohn H. N., Lugger P. M., Camilo F., Bogdanov S., Freire P. C., 2005, ApJ, 625, 796
Hooper D., Linden T., 2016, J. Cosmol. Astropart. Phys., 2016, 018
Hui C., Cheng K., Taam R. E., 2010a, ApJ, 714, 1149
Hui C., Cheng K., Wang Y., Tam P., Kong A., Chernyshov D., Dogiel V., 2010b, ApJ, 726, 100
Johnson T. J. et al., 2013, ApJ, 778, 106
Jones J. B. et al., 2006, AJ, 131, 312
Kelly B. C., 2007, ApJ, 665, 1489
Lee J.-W., Kang Y.-W., Lee J., Lee Y.-W., 2009, Nature, 462, 480
Liu C. et al., 2015, ApJ, 812, L2
Lloyd S. J., Chadwick P. M., Brown A. M., 2018, MNRAS, 480, 4782
Lorimer D., Kramer M., Ellis R., Huchra J., Kahn S., Rieke G., Stetson P., 2005, Handbook of Pulsar Astronomy, Cambridge Univ. Press, Cambridge
Lorimer D. R., 2001, Liv. Rev. Relat., 4, 5
Mattox J. R. et al., 1996, ApJ, 461, 396
McGlynn T., Scollick K., White N., 1998, in McLean B. J., , Golombek D. A., Hayes J. J. E.,, Payne H. E.,, eds, IAU Symp. 179, Skyview: The Multi-Wavelength Sky on the Internet., Kluwer Academic Publishers. p. 465
Michelson P. et al., 1994, ApJ, 435, 218
Mieske S. et al., 2004, AJ, 128, 1529
Mieske S., Hilker M., Infante L., 2002, A&A, 383, 823
Moore B., 1996, ApJ, 461, L13
Pooley D. et al., 2003, ApJ, 591, L131
Sandoval M. A. et al., 2015, ApJ, 808, L32
Sturrock P., 1971, ApJ, 164, 529

Tam P., Kong A., Hui C., Cheng K., Li C., Lu T.-N., 2011, ApJ, 729, 90
Tam P.-H. T., Hui C. Y., Kong A. K., 2016, J. Astron. Space Sci., 33, 1
Timmes F., Woosley S., Weaver T. A., 1995, ApJS, 98,
Verbunt F., 2003a, in Piotto G., Meylan G., Djorgovski S. G., Riello M., eds, ASP, San Francisco, CA, p. 245
Verbunt F., 2003b, ASP Conf. Ser. Vol. 296, Binary Evolution and Neutron Stars in Globular Clusters, Astron. Soc. Pac., San Francisco, p. 245
Verbunt F., Freire P. C., 2014, A&A, 561, A11
Wood M., Caputo R., Charles E., Di Mauro M., Magill J., Perkins J. S.; on behalf of the Fermi-LAT Collaboratio , 2017, Proc. Sci., Fermipy: An open-source Python package for analysis of Fermi-LAT Data, SISSA, Trieste, PoS(ICRC2017)824
Wu J., Hui C., Wu E., Kong A., Huang R., Tam P., Takata J., Cheng K., 2013, ApJ, 765, L47
Zhang P., Xin Y., Fu L., Zhou J., Yan J., Liu Q., Zhang L., 2016, MNRAS, 459, 99

APPENDIX: UPPER LIMITS AND TS RESIDUALS MAPS FOR NON-DETECTED GC

TS residual maps for all non-detected GCs are presented below, where the chosen test source was point-like, with an index 2 power-law spectrum. Maps presenting an isolated emission coincident with the optical position of a GC with $6 < TS < 25$ are shown in Fig. A1. These weak signals will probably be associated with GCs with a reasonable significance ($TS > 25$) within the next few years. All other non-detected GCs in the Milky Way presented $TS < 6$ or are surrounded by several point-sources with similar significance, making them hard to distinguish. These clusters are shown in Fig. A2. Energy flux upper limits with 95 per cent confidence levels and integrated over the whole analysis energy range are provided in Table A1, where the sources were assumed to have a power-law spectrum with a spectral index fixed at 2. A few of the sources described below are associated with globular clusters very close to the detection threshold in the preliminary LAT 8-year point source list [6] (FL8Y) and will likely be part of the 4th Fermi-LAT catalog (4FGL, in preparation). The reason why these sources have TS slightly above the threshold in FL8Y is likely related to the different likelihood method used for creating the catalogue (weighted likelihood).

The γ-ray spectra for 19 GCs, as discussed in Section 3.5, are shown in Fig. A3. The spectra of only 4 of the 23 detected clusters were not included, all of them due to problems with low statistics or difficult sky positions. The clusters detected with high significance in γ-rays are mainly dominated by a logparabola spectral shape, while for the low-significance ones, the logparabola model is not statistically preferred over a power-law. The spectra of 2MASS-GC01, Glimpse 01, and Glimpse 02 may have significant contamination from the Galactic diffuse emission, as these GCs are localized very close to the Galactic plane. The 19 spectra were obtained using the *fermipy* function *sed()*,[7] which computes the γ-ray spectra by performing independent fits for the flux normalization of a source in logarithmic spaced bins of energy (from 100 MeV up to 100 GeV in this case).

In Section 3.6, a linear regression was performed taking into account only the measurements of Γ and $N_{\rm MSP}$ (cf. Fig. 3a). In order to quantify the impact of the non-detections on the results, the Python port of the `LINMIX_ERR` package[8] was used. `LINMIX_ERR` is a Bayesian linear regression method that takes into account both measurement errors and non-detections (Kelly 2007). The fit incorporating upper limits is given by

$$\log N_{\rm MSP} = (2.17 \pm 0.55) \log \Gamma + (-2.86 \pm 1.07), \quad \text{(A1)}$$

which should be compared with the fit incorporating only measured values (cf. Section 3.6),

$$\log N_{\rm MSP} = (0.64 \pm 0.15) \log \Gamma + (0.80 \pm 0.20). \quad \text{(A2)}$$

Given that non-detections outnumber the detections by a factor of ∼7, it is not surprising that the two fits are considerably different from each other, as can be seen in Fig. A4. The fit involving only the detections is in good agreement with what is observed in X-rays and γ-rays for LMXBs and MSPs in previous works (Pooley et al. 2003; Abdo et al. 2010c; Hooper & Linden 2016), while the fit incorporating upper limits seems to underestimate the results in these works, giving a much lower number of MSPs per GC. This may be related to the high values of Λ found for many of these non-detections, which may diminish the expected γ-ray flux even if the source has a large value for Γ (see Section 3.7 for details).

[6] https://fermi.gsfc.nasa.gov/ssc/data/access/lat/fl8y/

[7] https://fermipy.readthedocs.io/en/latest/advanced/sed.html
[8] https://github.com/jmeyers314/linmix

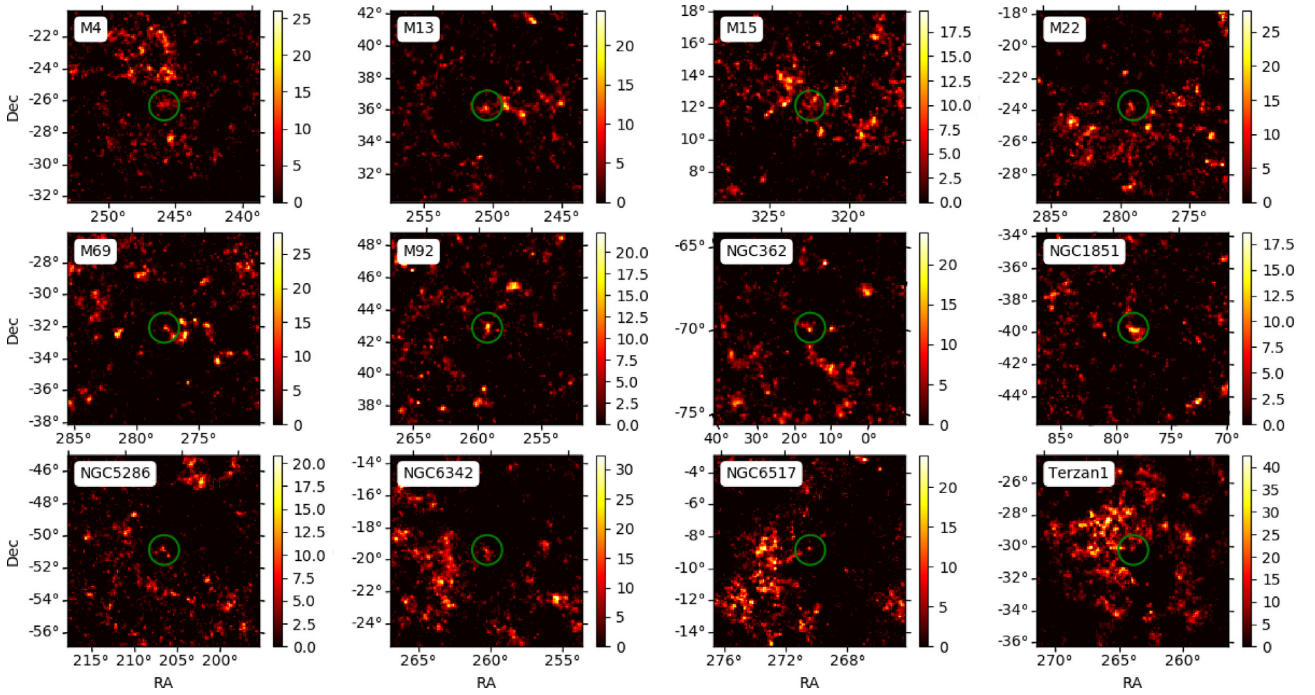

Figure A1. TS residual maps for sources that will be probably associated to GCs within a few years. Their emissions were modelled by power-laws and presented significances below 4σ. All maps are centred on the GCs positions given by the GLOBCUST catalogue. The green circles guide the readers to the centre of the maps.

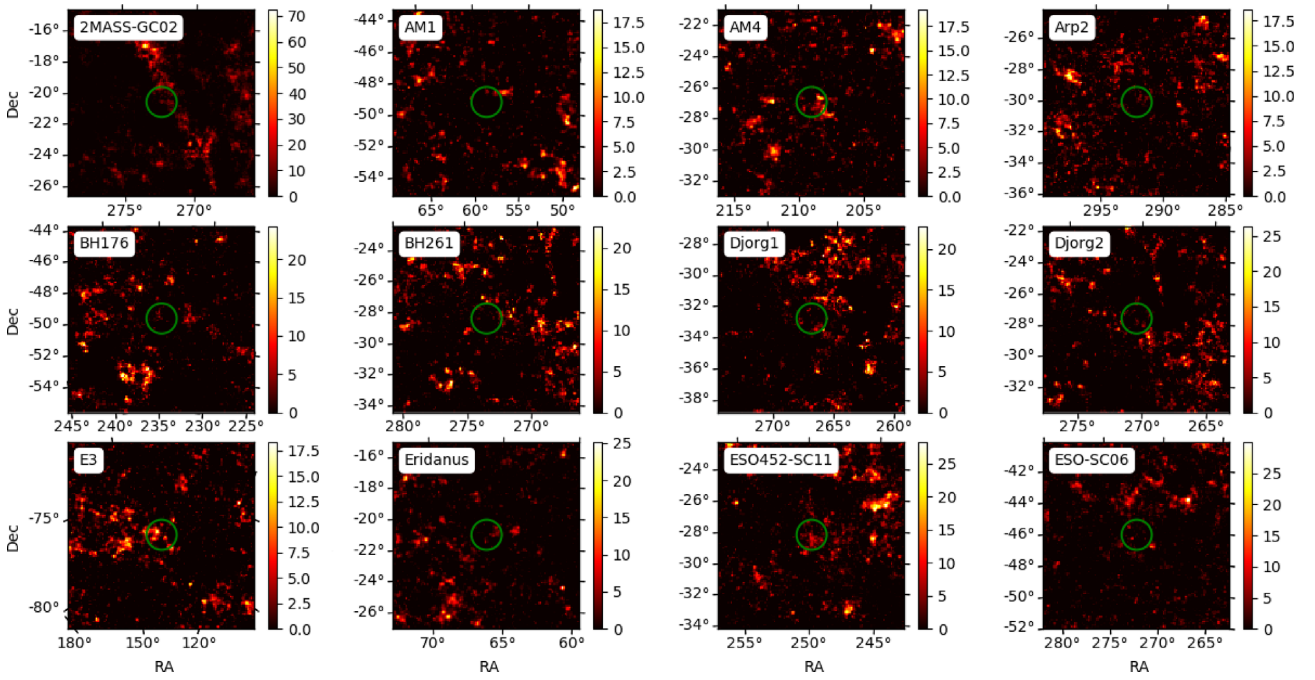

Figure A2. TS residual maps for all Milky Way GCs non-detected in γ-rays. All maps are centred on the GC positions given by the GLOBCUST catalogue. The green circles guide the readers to the centre of the maps.

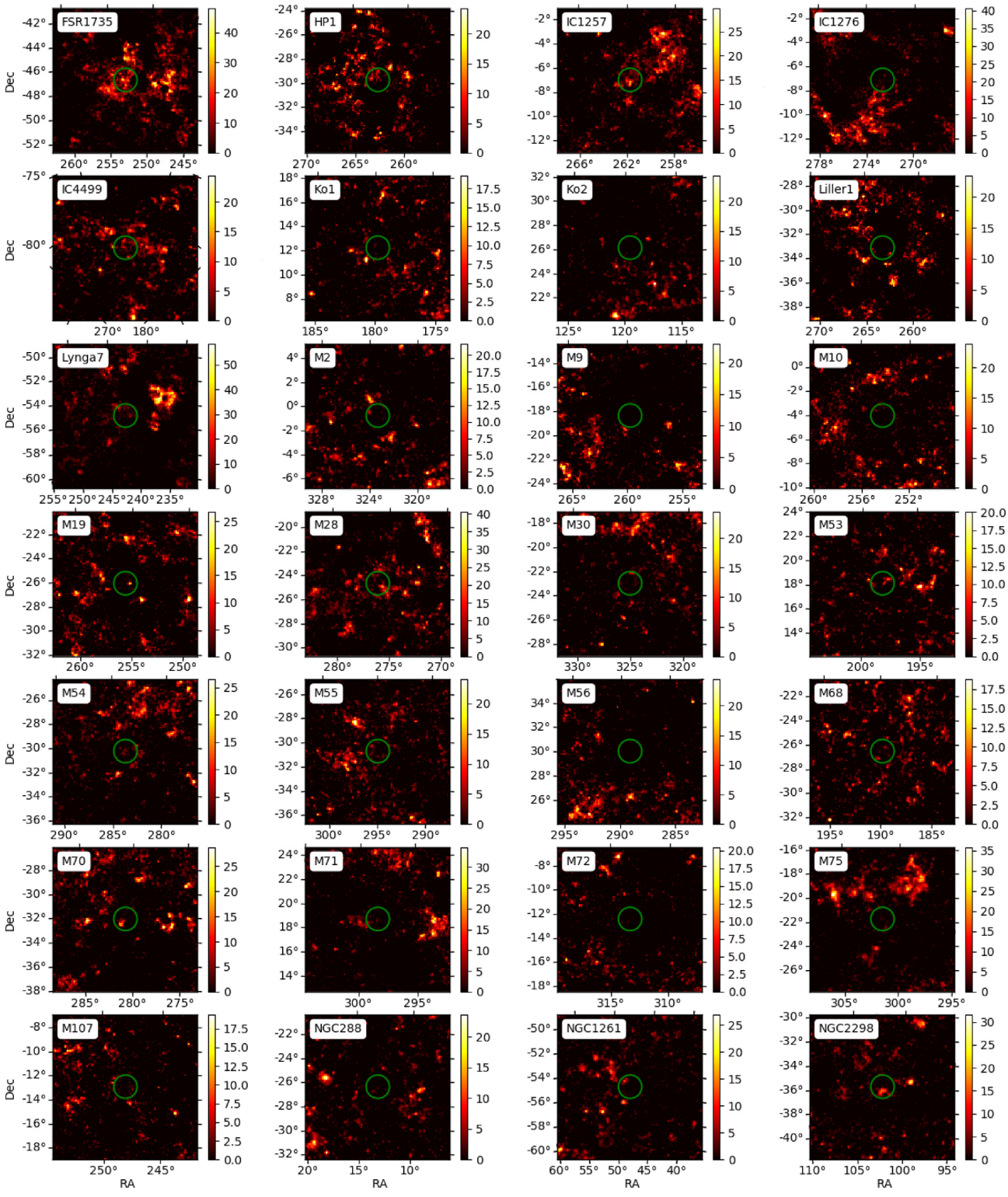

Figure A2 – *continued*

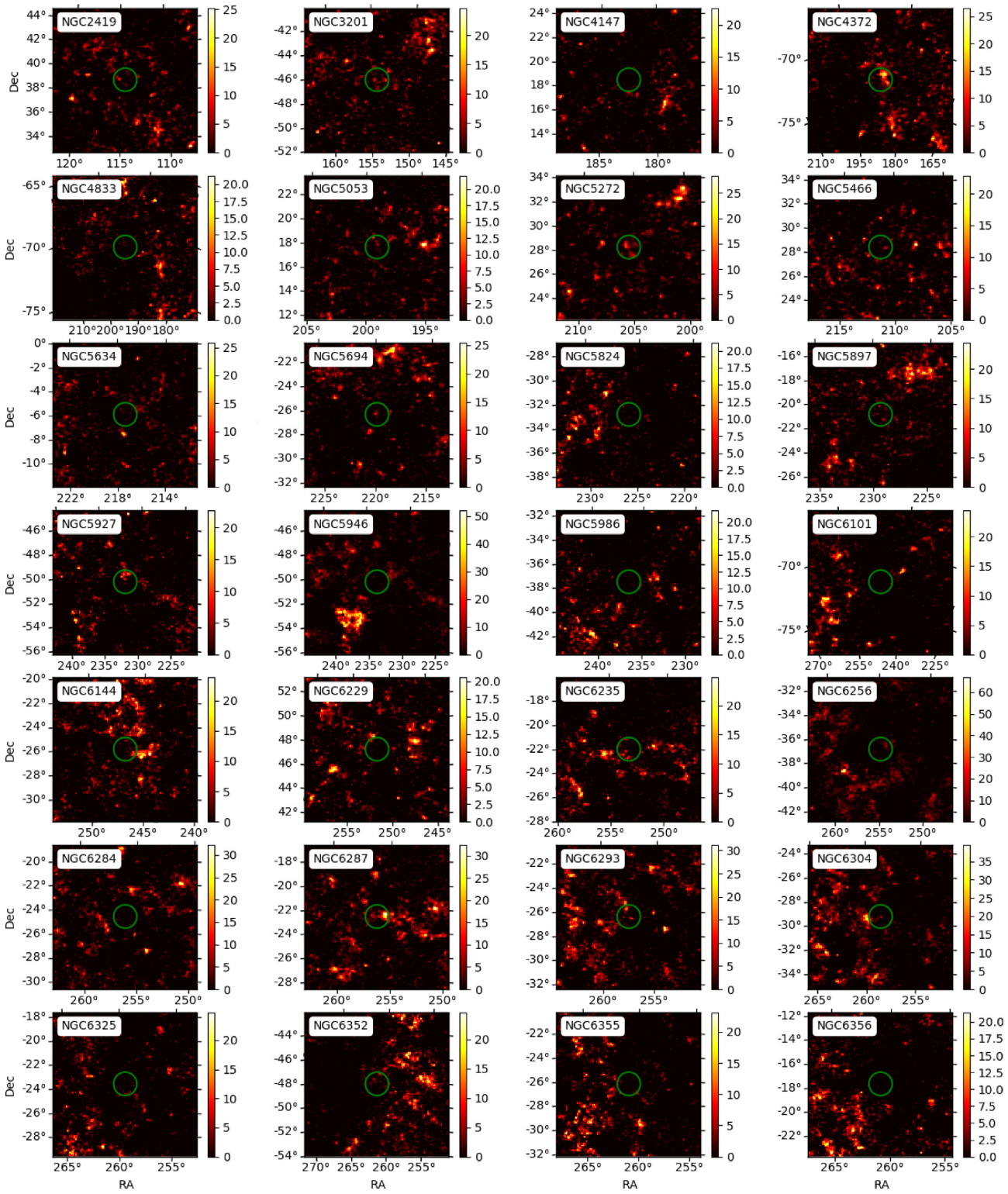

Figure A2 – *continued*

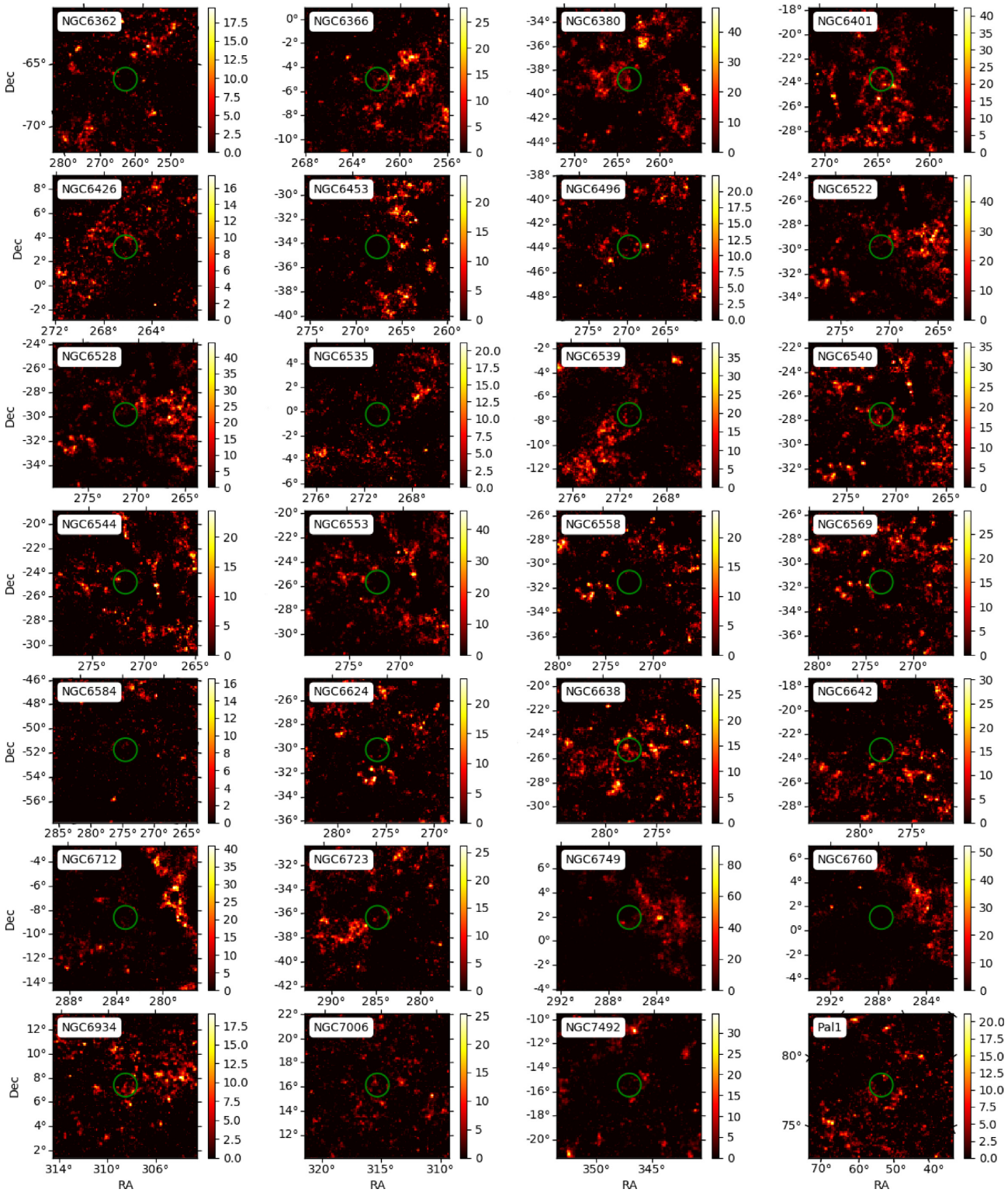

Figure A2 – *continued*

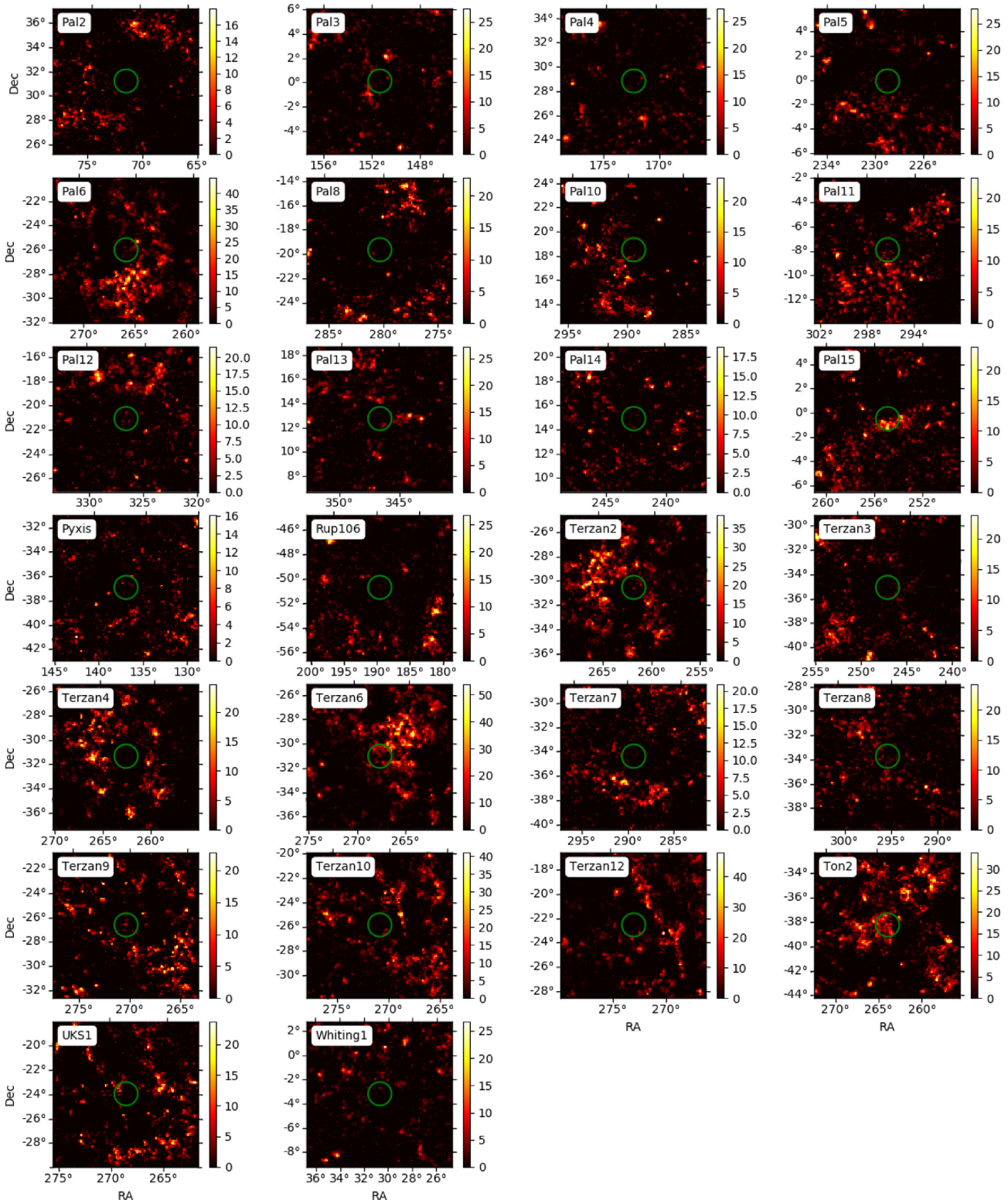

Figure A2 – *continued*

Table A1. Energyflux 2σ upper limits and TS values for all 129 GCs non-detected in γ-rays. The energy range adopted is from 100 MeV up to 100 GeV.

Cluster	Upper limit 10^{-13} er g cm^{-2} s^{-1}	TS
2MASS-GC02	129.6	18
AM1	32.0	0
AM4	20.3	5
Arp2	8.2	1
BH176	18.2	1
BH261	6.0	0
Djorg1	7.6	0
Djorg2	26.4	3
E3	13.1	4
Eridanus	5.7	0
ESO452-SC11	40.9	14
ESO-SC06	10.1	1
FSR1735	86.2	23
HP1	35.1	1
IC1257	41.1	14
IC1276	84.1	4
IC4499	22.2	7
Ko1	4.7	0
Ko2	1.7	0
Liller1	8.5	0
Lynga7	107.4	3
M2	6.1	0
M4	54.3	24
M9	1.7	0
M10	5.1	0
M13	32.3	23
M15	36.4	9
M19	10.5	0
M22	48.6	23
M28	47.1	4
M30	12.8	1
M53	18.7	5
M54	18.8	3
M55	23.2	6
M56	2.2	0
M68	18.6	14
M69	25.2	8
M70	17.2	4
M71	31.6	19
M72	1.5	0
M75	11.5	1
M92	32.3	18
M107	6.3	0
NGC 288	5.7	0
NGC 362	19.2	16
NGC 1261	10.4	7
NGC 1851	20.3	17
NGC 2298	28.8	14
NGC 2419	10.9	7
NGC 3201	17.4	3
NGC 4147	4.9	0
NGC 4372	35.1	10
NGC 4833	4.0	0
NGC 5053	9.5	1
NGC 5272	15.2	8
NGC 5286	35.6	15
NGC 5466	6.0	0
NGC 5634	3.6	0
NGC 5694	14.2	5
NGC 5824	3.3	0
NGC 5897	8.2	0
NGC 5927	12.5	0
NGC 5946	8.0	0
NGC 5986	3.7	0
NGC 6101	3.3	0
NGC 6144	6.3	0
NGC 6229	1.8	0
NGC 6235	4.9	0
NGC 6256	45.9	1
NGC 6284	2.1	0
NGC 6287	43.2	12
NGC 6293	15.7	1
NGC 6304	32.9	6
NGC 6325	7.9	0
NGC 6342	32.3	21
NGC 6352	6.4	0
NGC 6355	2.6	0
NGC 6356	2.2	0
NGC 6362	2.5	0
NGC 6366	20.8	2
NGC 6380	84.9	21
NGC 6401	128.4	11
NGC 6426	4.3	0
NGC 6453	3.0	0
NGC 6496	3.2	0
NGC 6517	34.6	6
NGC 6522	53.3	1
NGC 6528	54.1	3
NGC 6535	5.8	0
NGC 6539	11.3	0
NGC 6540	60.4	5
NGC 6544	12.1	0
NGC 6553	29.3	4
NGC 6558	2.2	0
NGC 6569	11.4	0
NGC 6584	2.3	0
NGC 6624	137.3	4
NGC 6638	48.9	5
NGC 6642	8.8	0
NGC 6712	17.8	6
NGC 6723	13.6	1
NGC 6749	113.9	0
NGC 6760	111.9	1
NGC 6934	17.7	7
NGC 7006	20.3	4
NGC 7492	9.5	1
Pal1	13.7	4
Pal2	2.1	0
Pal3	8.5	1
Pal4	2.8	0
Pal5	11.2	0
Pal6	3.00	5
Pal8	11.5	0
Pal10	3.1	0
Pal11	12.7	2
Pal12	4.8	0
Pal13	15.9	5
Pal14	3.0	0
Pal15	15.1	5
Pyxis	3.3	0
Rup106	13.9	2
Terzan1	99.7	18
Terzan2	42.2	8
Terzan3	3.4	0
Terzan4	2.9	0
Terzan6	129.7	14
Terzan7	8.4	0
Terzan8	21.1	4
Terzan9	40.8	5
Terzan10	34.2	5
Terzan12	3.4	0
Ton2	99.9	12
UKS1	7.3	0
Whiting1	2.0	0

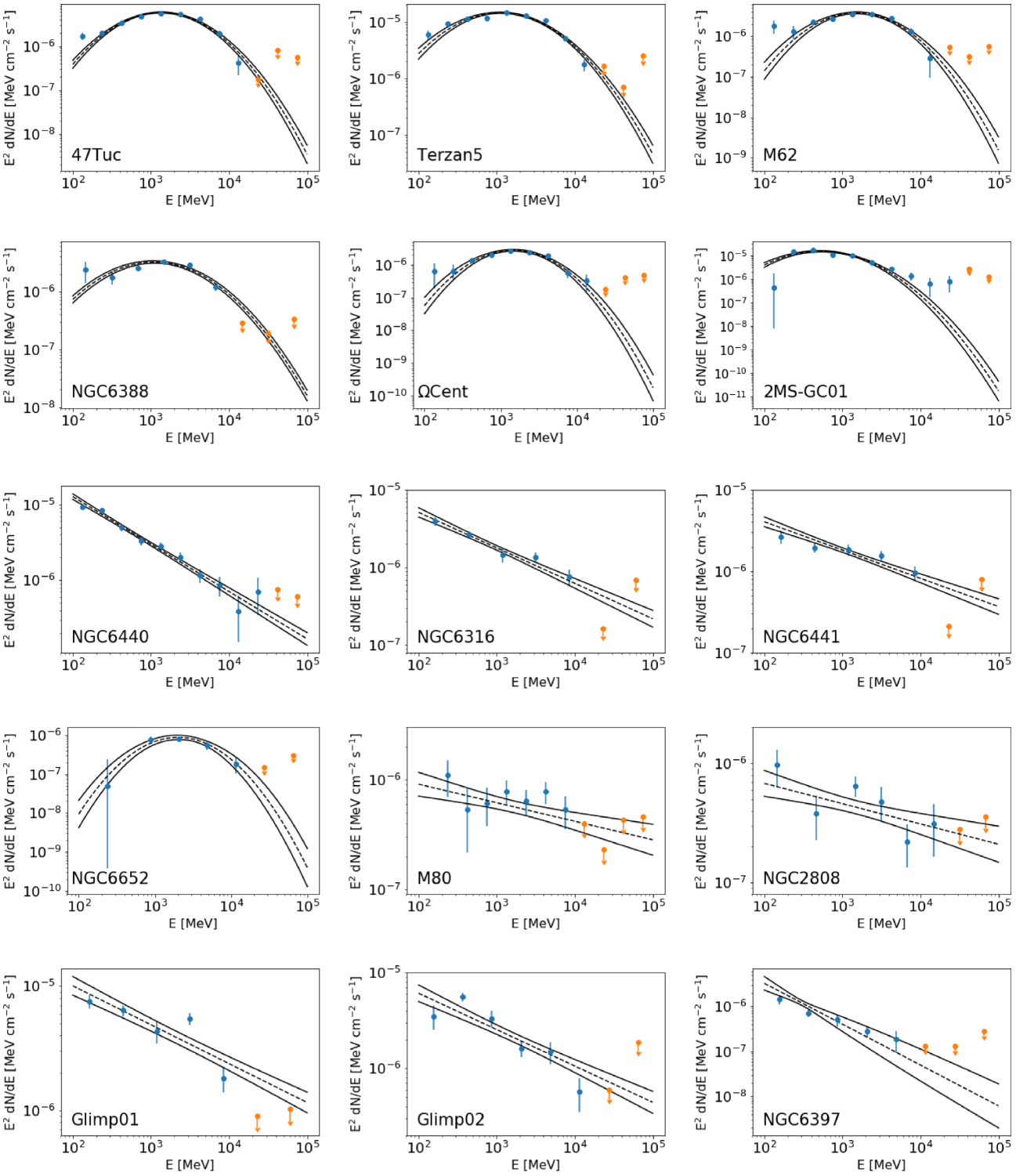

Figure A3. High-energy γ-ray spectra for 19 of the 23 γ-ray-bright GCs. The panels are organized accordingly with Table 1, with higher significance detections located in the top. All spectra are reasonably well fitted with a logparabola or power-law. It is easily noticeable the dominance of logparabola spectral shape between the most significant sources; the low-significance sources, on the other hand, are better described by a power-law. The adopted energy range was from 100 MeV up to 100 GeV.

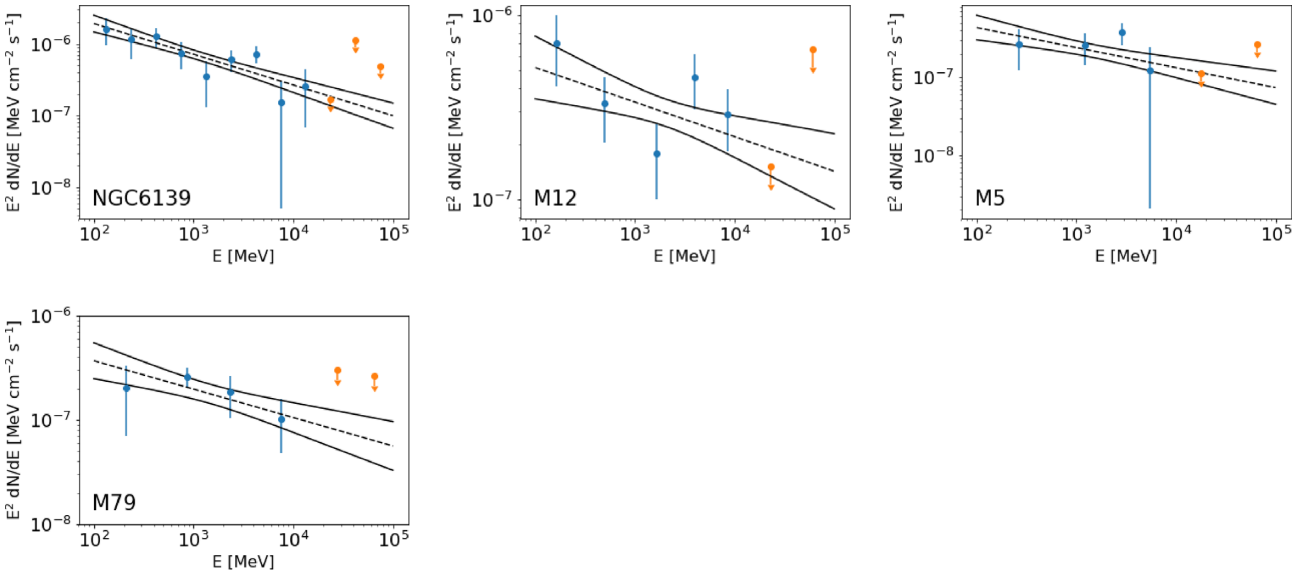

Figure A3 *– continued*

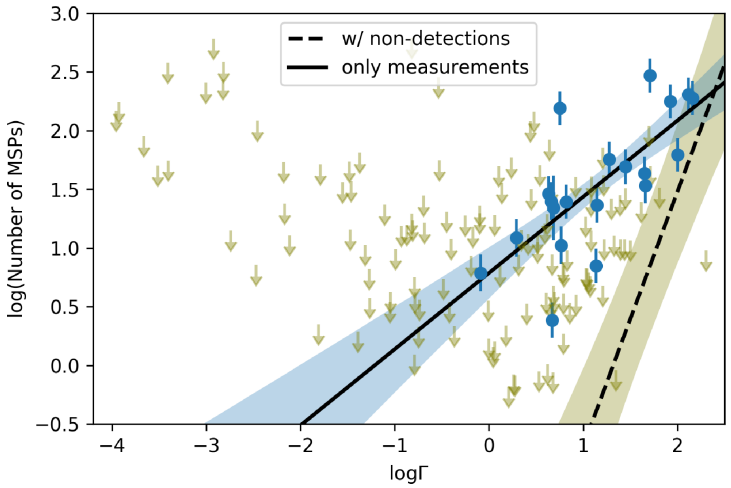

Figure A4. Linear regression for the number of MSPs and encounter rates. The solid line shows the fit to the data incorporating only actual measurements, while the dashed line takes into account measurements and non-detections (upper limits). The shaded regions around each line display the 1σ credibility bands for each fit.

This paper has been typeset from a TEX/LATEX file prepared by the author.